

The phase-space distribution of infalling dark matter subhalos

H.Y. Wang^{1,2} *, Y.P. Jing², Shude Mao³, Xi Kang²

¹*Center for Astrophysics, University of Science and Technology of China, Hefei, Anhui 230026, China*

²*Shanghai Astronomical Observatory, the Partner Group of MPI für Astrophysik, Nandan Road 80, Shanghai 200030, China*

³*University of Manchester, Jodrell Bank Observatory, Macclesfield, Cheshire SK11 9DL, UK*

Accepted Received; in original form

ABSTRACT

We use high-resolution numerical simulations to study the physical properties of subhalos when they merge into their host halos. An improved algorithm is used to identify the subhalos. We then examine their spatial and velocity distributions in spherical and triaxial halo models. We find that the accretion of satellites preferentially occurs along the major axis and perpendicular to the spin axis of the host halo. Furthermore, the massive subhalos show a stronger preference to be accreted along the major axis of the host halo than the low-mass ones. Approximate fitting formulae are provided for the physical properties of subhalos. Combined with analytical and semi-analytic techniques, these empirical formulae provide a useful basis for studying the subsequent evolution of subhalos and satellite galaxies in their hosts. Future studies should however account for satellites that may not be undergoing the first infall in their evolution.

Key words: large-scale structure of Universe - cosmology: theory - dark matter

1 INTRODUCTION

Cold Dark Matter (CDM) dominated cosmological models have received strong support from a wide range of observations (e.g., Spergel et al. 2003). In CDM models, the structures of dark matter are formed through the merger and accretion of smaller structures (White &

* whywang@mail.ustc.ac.cn, ypjing@shao.ac.cn, smao@jb.man.ac.uk, kangx@shao.ac.cn

Rees 1978). Dark matter halos are high-density structures that are a few hundred times of the mean background density and are in approximate dynamical equilibrium according to the virial theorem. Galaxies are expected to condense in dark matter halos due to dissipative cooling processes. The observable properties of the galaxies are thus strongly influenced by the hierarchical growth of their host halos. During the hierarchical assembly of the halos, smaller halos merged into bigger ones are found to be long-lived even though their outer part may be stripped by the tidal interactions (e.g., Tormen 1997; Klypin et al. 1999; Moore et al. 1999). Some of these subhalos are believed to be the hosts of the satellite galaxies in galactic-sized halos (such as the Milky Way) and of the galaxies in clusters of galaxies, therefore it is essential to understand the evolution and dynamics of these subhalos in galaxy formation. Indeed, it has been demonstrated that it is important to resolve the merger of subhalos in order to accurately predict the cluster luminosity function of galaxies (Springel et al. 2001) and the luminosity function of field galaxies (Kang et al. 2004). The presence of the subhalos was used to interpret the anomalous flux ratios of lensed quasar images (e.g., Mao & Schneider 1998; Kochanek & Dalal 2004), though it is still unclear if the amount of subhalos predicted by the CDM models is in quantitative agreement with the lensing observations (Mao 2004; Mao et al. 2004; Zentner et al. 2005a). In addition, the subhalos have important effects on the heating of galactic disks (Benson et al. 2004) and possible γ -ray emission from annihilation of dark matter particles (Taylor & Silk 2003; Stoehr et al. 2003; see Bertone et al. 2004 for a review.)

Because of the importance of the subhalos in cosmological studies, there have been many high-resolution N-body studies of subhalos since Moore et al. (1999) who discovered that subhalos can survive within bigger halos for a significant period of time. The mass function of subhalos was shown to be proportional to $\sim (M_{\text{sub}}/M_{\text{host}})^{-1.8}$ (e.g., Klypin et al. 1999; Moore et al. 1999; Ghigna et al. 2000), and the radial distribution of subhalos above a given mass is much flatter than that of the dark matter in the host halo (e.g., Gao et al. 2004a; Diemand et al. 2004; Mao et al. 2004). The velocity dispersion of the subhalos is larger than that of the underlying dark matter (positive velocity bias), except in the innermost region where the velocity anti-bias is found for the subhalos (Ghigna et al. 1998; Okamoto & Habe 1999; Colin et al. 2000; Klypin et al. 1999; Springel et al. 2001; Diemand et al. 2004). In their recent work, Gao et al. (2004a) showed that most present-day subhalos identified in their simulations have been accreted into their host halos very recently. This indicates that the subhalos accreted earlier, even if they were massive enough to host bright galaxies, may have

been disrupted in the current generation of high-resolution simulations (Gao et al. 2004b) due to physical (such as tidal stripping) and numerical effects (e.g., limited resolution). It is therefore very demanding resolution-wise to correctly model the dynamics, mergers and evolution of subhalos and satellites in the densest regions (Kang et al. 2004), and thus an analytical theory would be preferred to follow the evolution of subhalos within their hosts.

Indeed, parallel to the numerical studies, significant progress has been made in understanding the evolution and the distribution of subhalos with analytical models (e.g., van den Bosch et al. 1999; Klypin et al. 1999; Taylor & Babul 2002, 2004; Sheth 2003; Zentner & Bullock 2003; Ougri & Lee 2004; van den Bosch, Tormen & Giocoli 2005). The two principal physical processes, dynamical friction and tidal stripping, which determine the evolution of subhalos, are relatively well understood. However, as noted by Benson (2005), the initial conditions (velocities and positions) of the infalling subhalos adopted in these studies are not from the prediction of hierarchical CDM models. Although some of these studies predicted subhalos with physical properties in reasonable agreement with those found in simulations, their success depends in part on the fine-tuning of the model parameters, such as the Coulomb logarithm function in the dynamical friction formula (e.g., Ougri & Lee 2004). Obviously, in order to make such an analytical approach more useful for studying the evolution of subhalos and satellite galaxies, it is a prerequisite to use the correct initial phase space information of the infalling subhalos as found in the CDM cosmological model.

Several authors have already studied the orbital parameters of the subhalos at the time of their mergers with the host halo (Tormen 1997; Vitvitska et al. 2002; Khochfar & Burkert 2004; Benson 2005). Tormen (1997) and Khochfar & Burkert (2004) used high-resolution re-simulations of halos and identified the progenitors of these halos. The orbital distribution is then measured from the progenitors that are about to merge with the main progenitor. In contrast, Vitvitska et al. (2002) and Benson (2005) identified pairs of halos that are about to merge, and measured the orbital distribution of these pairs. Among these studies, Benson (2005) used a large set of cosmological simulations provided by the Virgo Consortium (Jenkins et al. 2001), and formed a large sample of such orbital pairs. From this, he presented fitting formulae for the distribution of the initial infall velocity of the subhalos at the virial radius of their host halo.

Although the work of Benson (2005) is an important step forward to determine the initial condition of infall subhalos, there is an important question yet to be examined quantitatively, i.e., whether the mergers are isotropic in the position space or there is some preferential di-

rection for the mergers. Earlier studies suggest the accretion is anisotropic (e.g., Tormen 1997). For example, Aubert, Pichon & Colombi (2004) found the infall takes place preferentially in the plane perpendicular to the direction defined by the spin of the halo. In this paper, we use a cosmological N-body simulation of 512^3 particles (Jing & Suto 2002; Kang et al. 2004) to investigate this problem in more detail. As we will show, the mergers are preferentially along the major axis of the host halos; we will quantify this anisotropic accretion as a function of the subhalo mass (see also Libeskind et al. 2005). Compared with the simulations used by Benson (2005), our simulation has higher force and mass resolutions, and the subhalos are better resolved. This makes it easier and more reliable to quantify the orbital distribution of subhalos. This is particularly important for small subhalos as they may lose their identities in low resolution N-body simulations when they are close to the boundary of bigger halos. It is difficult to account for this population of missing subhalos if only one snapshot of the simulation output is used.

The paper is structured as follows. In §2, we briefly describe the numerical simulations we use, and how the subhalos are identified. In §3, we study the physical properties of subhalos and present simple empirical fitting formulae to these properties. In §4 we summarize our main results and discuss areas for future improvement.

2 N-BODY SIMULATION

The simulation used in this paper is a P³M cosmological simulation of 512^3 particles in a box of $100 h^{-1}\text{Mpc}$. The cosmological model is the standard concordance model with the density parameter $\Omega_{\text{m},0} = 0.3$, the cosmological constant $\Omega_{\Lambda,0} = 0.7$ and the Hubble constant $h = H_0/(100 \text{ km s}^{-1} \text{ Mpc}^{-1}) = 0.7$. The initial density field is assumed to be Gaussian with a Harrison-Zel'dovich primordial power spectrum and with an amplitude specified by $\sigma_8 = 0.9$, where σ_8 is the r.m.s. fluctuation of the linearly evolved density field in a sphere of radius $8 h^{-1}\text{Mpc}$. This simulation, which started at redshift $z_i = 72$, is evolved by 5000 time steps to the present day ($z = 0$) with our vectorized parallel P³M code (Jing & Suto 2002). The force softening length η_f (S2 type, Hockney & Eastwood 1981) is $10 h^{-1}\text{kpc}$ comoving, and the particle mass $m_p = 6.2 \times 10^8 h^{-1}M_{\odot}$. Because these simulation parameters are very similar to those adopted in many high-resolution re-simulations of individual cluster halos (Moore et al. 1999, Jing & Suto 2000, Fukushige & Makino 2001, 2003, Power et al. 2003,

(Diemand et al 2004), we have achieved a resolution that can resolve subhalos within massive host halos.

The dark matter halos are identified at redshift $z = 0$ in the simulation described above using the Friends-of-Friends method (FOF) with a linking length equal to 0.2 of the mean particle separation. The subhalos are then identified within the FOF halos with the SUBFIND routine (Springel et al. 2001). In Kang et al. (2004), the mass function of the subhalos was examined, and was found to be in good agreement with the subhalo mass functions obtained in previous halo re-simulations (Springel et al. 2001) down to a mass of about $3.1 \times 10^{10} h^{-1} M_{\odot}$ (50 particles). This indicates that the subhalos with more than $N_{\text{sub}} = 50$ particles are resolved in the simulation. Considering the fact that subhalos can survive more easily in the outskirts than in the inner dense region of a host halo, we relax the lower limit to 20 particles for the subhalo mass. Table 1 lists the number of particles we use to identify the subhalos and halos in several different combinations. And we only use the simulation output at $z=0$ to calculate the distribution.

3 RESULTS

3.1 The phase-space distribution in the spherical halo model

We first consider the density profile of host halos as a sphere and search for subhalos within a spherical shell with radius r between $1 - \Delta r$ and $1 + \Delta r$, where r is the distance between the centres of the subhalo and the host halo in units of the virial radius r_{vir} of the host halo. We identified the ‘‘centres’’ of the halos as the lowest-potential particles using the SUBFIND routine (Springel et al. 2001; Kang et al. 2004); we also checked that the ‘‘centre’’ identified this way is very close to the centre of mass for most host halos. We normally take the thickness of the shell (Δr) to be 0.1 or 0.2 (see Table 1). The virial radius is determined according to the spherical collapse model (Kitayama & Suto 1996; Bryan & Norman 1999). In this section, we consider only those subhalos with an inward directed velocity. We treat the subhalos and host halos as point-mass particles, and determine the velocity of the subhalos at the time when their orbits first cross the virial radius of the host halo under gravity. We also compute the time t_{cr} for each subhalo to cross from $1 + \Delta r$ to $1 - \Delta r$ according to their trajectories. Subhalos with a larger t_{cr} will stay longer in the shell of $1 \pm \Delta r$ than those with smaller t_{cr} . During a time interval dt , the chance of observing this subhalo within the spherical shell will be dt/t_{cr} . Thus we weight each subhalo by t_{cr}^{-1} when we compute the

distributions of position, radial and tangential velocities. We will excise the subhalos that do not pass through one or both of the radial limits.

The distributions of the radial (v_r) and tangential (v_θ) velocities of these subhalos are presented in Fig. 1; both velocities are in units of the circular velocity at the virial radius, v_{vir} . For this exercise, we only retain host halos with more than 500 particles and subhalos with more than 20 particles, corresponding to the selection parameter set A in Table 1. The v_r distribution peaks around the virial velocity, while v_θ peaks at a slightly smaller value, around 0.7. Both distributions drop essentially to zero beyond 1.5 virial velocity. The shape of these distributions qualitatively agrees with that obtained by Benson (2005). Quantitatively, however, both distributions appear slightly broader than those in Benson (2005). We do not know the exact reason for the difference, but it may be attributed to the different ways of selecting the subhalos. For low resolution simulations, subhalos close to the inner shell $1 - \Delta r$ may be difficult to identify with the friends-of-friends or the spherical overdensity methods. Benson (2005) attempted to correct for this effect by considering a minimum radius at which the subhalo can still be identified using his algorithm. With the SUBFIND routine (Springel et al. 2001), we are able to resolve the subhalos even when they are quite close to the host halos, so we do not need to make this complicated correction. Instead we simply consider all the subhalos within the spherical shell between radius $1 - \Delta r$ and $1 + \Delta r$.

A related quantity to v_r and v_θ is the infall angle, defined as

$$\cos \alpha_{\text{infall}} = \frac{v_r}{(v_r^2 + v_\theta^2)^{1/2}}. \quad (1)$$

For a radially infalling subhalo $\alpha_{\text{infall}} = 0$. The distribution of α_{infall} is shown in the bottom left panel. The infall angle has a peak around 35° , and a full-width-at-half-maximum of about 50° .

It is well known that halos accrete matter along the large-scale filaments that connect the halos, this implies that the merger of the subhalos into the host halos may be anisotropic (Lee, Jing, & Suto 2005). Since the halos are generally triaxial (Jing & Suto 2002), there could be a correlation between the direction of the subhalo merger and the shape of the host halo. We therefore determine the three principal axes for each halo from its inertial tensor within the virial radius. We define θ to be the angle between the major axis of the host halo and the vector from the host halo centre to the centre of a subhalo, and ϕ as the other polar angle ($0 \leq \phi < 2\pi$). Because of the limited sample size, we will focus on the

spatial distribution as a function of μ ($\equiv |\cos\theta|$), despite of the fact the distribution also depends on ϕ but more weakly than on θ . The probability distribution of μ , $df/d\mu$, for the subhalos is shown in the lower right panel of Fig. 1. If the subhalos merge into the host halo isotropically, then we expect $df/d\mu$ to be unity. In contrast to this expectation, $df/d\mu$ of the subhalos increases strongly with μ , implying that subhalos are accreted more preferentially along the major axis of the host halos.

Since dark halos are triaxial (Jing & Suto 2002), the dark matter density at the spherical virial radius is expected to be higher in the direction of the halo major axis. If the spatial distribution of subhalos follows that of the dark matter, we would expect a higher $df/d\mu$ in the direction of $\mu = 1$. The question is whether the increase of $df/d\mu$ with μ can be fully explained by the shape of host halos. In the following subsection, we examine this question, i.e., consider the phase space distribution in the ellipsoidal coordinate system in the more realistic triaxial halo model.

3.2 The phase-space distribution in the triaxial halo model

For each host halo, we determine the axial ratios a/c and b/c from their inertia tensor within its virial radius r_{vir} , where a , b , and c are the minor, median, and major axes of the halo respectively. If we rotate the coordinate (x, y, z) so that the new X , Y and Z coordinate axes are parallel to the minor, median, and major axes of the halo, the isodensity surfaces of a halo are approximately described by (Jing & Suto 2002)

$$R^2 = \frac{c^2 X^2}{a^2} + \frac{c^2 Y^2}{b^2} + Z^2. \quad (2)$$

We define the boundary of an ellipsoidal halo R_{vir} such that the total mass within R_{vir} is equal to the virial mass of the halo in the spherical model. We then examine the orbital parameters and density of the subhalos at this surface. In analogy with the previous subsection, we take a shell of the upper and lower ellipsoidal radii $(1 \pm \Delta R)$ in units of R_{vir} , and compute the distributions of the normal and tangential velocities (v_n and v_t) relative to the ellipsoidal surface as well as the number density distribution. In this exercise, we only include the subhalos that have an inward directed velocity. The infall angle α_{infall} can be similarly defined as in eq. (1) with v_r and v_θ replaced by v_n and v_t .

The results are given in Fig. 2. The distributions of the normal and tangential velocities are very similar to those in spherical shells in the previous subsection. The subhalo number density $n_{\text{tri}}(\mu)$, which is the density averaged over ϕ directions for a fixed μ on the surface

R_{vir} , is shown as a function of μ in the middle right panel. Notice that in the triaxial halo model, a flat distribution in μ implies that the subhalos follow the idealised ellipsoidal shape. As expected, the dependence on μ becomes significantly weaker in the ellipsoidal shells, but there is still a preference for the subhalos to merge into their host halos along the major axis. To facilitate comparisons with previous studies, we also show in Fig. 2 (bottom two panels) the distributions of the total velocity $v = (v_n^2 + v_t^2)^{1/2}$, and the orbital ‘circularity’ $\epsilon \equiv J/J_c$, where J is angular momentum and J_c is the angular momentum of a circular orbit with the same energy. The orbital circularity has a broad peak around 0.5, indicating the infall is in neither purely radial nor tangential orbits. This result is in good agreement with previous studies (e.g., Tormen 1997, Fig. 4; Ghigna et al. 1998, Fig. 14).

Next we examine the distribution of the velocities as a function of the angular positions of the subhalos relative to the major axis of the ellipsoidal host halo. To do this, we divide the ellipsoid into three equal bins in $0 \leq \mu \leq 1$. In Fig. 3, we show the distributions of the normal and tangential velocities for these three bins. The distributions are quite similar. The bottom two panels show the mean total velocity and the mean infall angle as a function of μ . Again these two quantities have little dependence on μ . Therefore we can use the distributions as shown in Figure 2 to more accurately describe the distribution of the subhalo velocities.

We have also studied the distributions as a function of halo mass. For this purpose, we increase the lower limit of the host halos to 5000 particles ($3.1 \times 10^{12} h^{-1} M_\odot$) which corresponds to the halo selection parameter set C in Table 1. The results are compared with those of the host halos with parameter set B, where we included host halos with more than 500 particles. To increase the number of subhalos in the case of C, we have adopted $\Delta r = 0.2$. As shown in the two bottom panels of Figure 3, we found the statistical distributions change very little with reasonable changes of Δr . Figure 4 shows the results. No significant difference can be found for the two velocity distributions and the infall angle distribution. However, the number density dependence on μ becomes weaker when we increase the lower limit of the host halo mass and hence include more subhalos with smaller $M_{\text{sub}}/M_{\text{host}}$. If the smaller subhalos follow more closely the triaxial density profile, then the trend seen in Fig. 4 can be understood because the mass density should follow the triaxial density model.

To see the preferential accretion of more massive subhalos along the major axis, in Fig. 5 we divide the subhalos in six bins of $M_{\text{sub}}/M_{\text{host}}$ (with roughly equal numbers) and show their distributions of μ . The mass bins are listed in Table 3. The lowest mass-bin subhalos have only a weak dependence on μ , indicating that they are roughly consistent with the

triaxial shape. However, the highest mass subhalos (top left panel) with $M_{\text{sub}}/M_{\text{host}} \gtrsim 0.08$ shows dramatic deviation from the ellipsoidal accretion, with a strong peak around $\mu = 1$ (i.e., $\theta = 0^\circ$). Fig. 5 clearly illustrates that more massive subhalos are accreted with a much stronger preference along the major axis of the host halo. This may have observable consequences for the satellite galaxies we see today; we return to this important point briefly in the discussion.

We have shown that the infall of subhalos are preferentially along the major axis of the parent halo determined by the moment of inertia. An alternative way of defining the orientation of a halo is using its spin axis, which can be defined by the total angular momentum of the particles within the virial radius. Aubert, Pichon & Colombi (2004) found that the infall takes place preferentially in the plane perpendicular to the direction defined by the spin of the halo. Fig. 6 shows the distribution of the angle between the spin axis and the line connecting the centres of the parent halo and the satellite in our simulation. Clearly there is a (weak) preference for satellites to be perpendicular to the spin axis, in agreement with the findings of Aubert et al. (2004, see their Fig. 8, which is based on a more sophisticated spherical harmonics analysis). This is to be expected as the spin axis is statistically perpendicular to the major axis of the halo, as shown by previous studies (e.g. Warren et al. 1992, Dubinski 1992).

Many analytical models of the subhalo population require an accurate knowledge of the initial conditions for the subhalos. In the following, we provide empirical fitting formulae found in our numerical simulations. To facilitate comparisons with Benson (2005), we adopt the same functional forms to fit the velocity distribution, specifically,

$$f(v_n, v_t) = a_1 v_t \exp[-a_2(v_t - a_9)^2 - b_1(v_t)\{v_n - b_2(v_t)\}^2] \quad (3)$$

where

$$b_1(v_t) = a_3 \exp[-a_4(v_t - a_5)^2], \quad (4)$$

$$b_2(v_t) = a_6 \exp[-a_7(v_t - a_8)^2]. \quad (5)$$

The fitted curves are shown in Fig. 2, and the fit parameters are listed in Table 2. We also use the following function

$$df/d\mu = p_0 + p_1 \exp(p_2 \mu^2), \quad \mu \equiv \cos \theta, 0 \leq \mu \leq 1 \quad (6)$$

to describe the angular distribution of the subhalo accretion. The function has two parameters, p_1 and p_2 , and p_0 is chosen such that the function is properly normalised when μ is

integrated from 0 to unity. The fit parameters are listed in Table 3. As can be seen, the fitting functions match our simulation results quite well.

4 DISCUSSIONS

We have used a high-resolution simulation to study the initial conditions of subhalos when they merge into their host halos. Most of our results are in good agreement with Benson (2005). One finding of our study is that massive subhalos are accreted more preferentially along the major axis of the host halos than the less massive ones. Our subhalos are identified at present day ($z = 0$), but the same trend for massive subhalos should apply at high redshifts (Kravtsov et al. 2004). If the more massive subhalos house satellite galaxies and they survive until the present day, then the satellites should show a more planar geometry along the major axis. Interestingly, the satellite galaxies in the Milky Way appear to lie in a great disk (Kroupa et al. 2005; see also Willman et al. 2004), almost perpendicular to the stellar disk. If the major axis of the dark matter halo is perpendicular to the stellar disk in the Milky Way, then such a distribution, while puzzling at first, is naturally expected in the CDM (Kang et al. 2005; Libeskind et al. 2005; Zentner et al. 2005b).

Our result that more massive subhalos are more preferentially accreted along the major axis of the host halo can be understood in the cosmic web theory (Bond, Kofman, & Pogosyan 1996; Lee, Jing, & Suto 2005). In this theory, the coherence of the initial tidal field forms one dimensional filaments. The halos are bridged by the filaments, and the merger of halos is expected to occur along the filaments. If the major axis of host halos is determined by the neighboring massive filaments, we would expect subhalos to merge preferentially along the major axis. A quantitative computation is possible for the distribution of $df/d\mu$ following Lee et al. (2005) which will be explored in a future work.

The initial conditions we found can be used in analytical formalisms (e.g., Oguri & Lee 2004; Taylor & Babul 2004) to predict the subsequent evolutions of subhalos and compare these with observations. Our results make it straightforward to generate Monte Carlo realizations of the subhalo population. The extended Press & Schechter formalism accurately predict the mass function of the subhalos. For a given halo, the triaxial halo shape can be sampled using Monte Carlo with the fitting formulae given by Jing & Suto (2002). The velocities of the halo can then be obtained using eq. (3). To describe the angular position of the satellite, the polar angles (θ, ϕ) are needed. To the first order, the polar angle (ϕ) is

approximately uniformly distributed between 0 to 2π . The angle θ can be generated using eq. (6). The mass dependence of the angle θ can be properly taken into account by choosing different fit parameters (in Table 3) depending on the value of $M_{\text{sub}}/M_{\text{host}}$.

In this paper we have analyzed the phase-space information of subhalos located in a thin shell close to the virial radius. In practice, we found that about 30% of subhalos within the shell have outgoing velocities. Some of these subhalos and perhaps even some inward moving subhalos could have been inside the host halo already, thus some of these subhalos could have evolved dynamically within the host halo and their phase-space information cannot be regarded as “initial” conditions. The number of secondary infall halos can be crudely estimated as follows. Let us approximate the parent halo as spherical, and assume that there are N subhalos falling into the parent halo for the first time. Due to symmetry, we can assume all subhalos move along the positive x -axis, and a fraction f of the subhalos will emerge as outgoing subhalos on the opposite side of the halo. Presumably all these fN subhalos will be accreted again in a second infall, and some fraction (presumably $\lesssim f$) of these subhalos will emerge as outgoing ones on the positive x side. So in total there are $N + fN$ infall subhalos, and $fN + f^2N$ outgoing subhalos. The ratio of infalling and outgoing subhalos is therefore $(N + fN)/(fN + f^2N) \approx 7/3$, implying $f \sim 3/7$. Hence the fraction of the secondary infall subhalos is about $fN/(N + fN) \lesssim 30\%$. Gill et al. (2005) investigated satellite galaxies in the outskirts of galaxy clusters from their high-resolution simulations (see also Gill et al. 2004a,b). They found that approximately one half of the galaxies with current cluster-centric distance in the interval 1-2 virial radii of the host are ‘backsplash’ galaxies that once penetrated the cluster potential. If one half of these ‘backsplash’ galaxies have negative radial velocities, then this suggests that the fraction of subhaloes undergoing secondary infall is about $\sim 25\%$, consistent with our estimate above.

To more properly account for this population of evolved subhalos in detail, one must track the subhalos as a function of redshift. This will also be useful for studying the time evolution of initial conditions. Another issue not studied in detail here is the ϕ dependence of the subhalo spatial distribution. This quantity is taken to be uniform between 0 to 2π , while approximately correct to the first order, a more realistic treatment is desirable. We plan to return to these issues in future works.

ACKNOWLEDGMENTS

We thank the referee for a helpful report which improved the paper. The research is supported by NKBRFSF (G19990754), NSFC (Nos. 10125314, 10373012), and Shanghai Key Projects in Basic research (No. 04jc14079). SM acknowledges the financial support of Chinese Academy of Sciences and the European Community's Sixth Framework Marie Curie Research Training Network Programme, Contract No. MRTN-CT-2004-505183 "ANGLES". HYW and SM wish to thank the hospitality of Shanghai Astronomical Observatory during several scientific visits.

REFERENCES

- Aubert D. Pichon C. Colombi S., 2004, MNRAS, 352, 376
- Benson A. J., 2005, MNRAS, 358, 551
- Benson A. J., Lacey C. G., Frenk C. S., Baugh C. M., Cole, S. MNRAS, 2002, 351, 1215
- Bertone G., Hooper D., Silk J., 2004, Phys. Rep. 405, 279
- Bond J., R., Kofman L., Pogosyan D., 1996, Nature, 380, 603
- Bryan G. L., Norman M. L., 1998, ApJ, 495, 80
- Colín P., Klypin A. A., Kravtsov A. V., 2000, ApJ, 539, 561
- Diemand J., Moore B., Stadel J. 2004, MNRAS, 352, 535
- Dubinski J., 1992, ApJ, 401, 441
- Gao L., De Lucia G., White S. D. M., Jenkins A., 2004a, MNRAS, 352, L1
- Gao L., White S. D. M., Jenkins A., Stoehr F., Springel V., 2004b, MNRAS, 355, 819
- Ghigna S., Moore B., Governato F., Lake G., Quinn T., Stadel J., 1998, MNRAS, 300, 146
- Ghigna S., Moore B., Governato F., Lake G., Quinn T., Stadel J., 2000, ApJ, 544, 616
- Gill S. P. D., Knebe A., Gibson B. K. 2004a, MNRAS, 351, 399
- Gill S. P. D., Knebe A., Gibson B. K., Dopita A. D., 2004b, MNRAS, 351, 410
- Gill S. P. D., Knebe A., Gibson B. K., 2005, MNRAS, 356, 1327
- Hockney R. W., Eastwood J. W., 1981, Computer Simulation Using Particles (New York: McGraw-Hill)
- Jing Y. P., Suto Y., 2002, ApJ, 574, 538
- Kang X., Jing Y. P., Mo H. J., Börner G., 2004, ApJ, in press (astro-ph/0408475)
- Kang X., Mao S., Gao L., Jing Y. P., 2005, A&A, 437, 383
- Kitayama T., Suto Y., 1996, ApJ, 469, 480
- Klypin A., Kravtsov A. V., Valenzuela O., 1999, ApJ, 522, 82
- Kravtsov A. V., Gnedin O. Y., Klypin A. A., 2004, ApJ, 609, 482
- Khochfar S., Burkert A., 2004, MNRAS, submitted (astro-ph/0309611)
- Kroupa P., Theis C., Boily C. M., 2005, A&A, 431, 517
- Kochanek C.S., Dalal N., 2004, ApJ, 610, 69
- Lee J., Jing Y.P., Suto Y., 2005, ApJ, in press
- Libeskind N. I., Frenk C. S., Cole S., Helly J. C., Jenkins A., Navarro J. F., Power C., 2005, astro-ph/0503400
- Mao S., 2004, IAU 220, Eds. M. A. Walker, & K. C. Freeman. ASP 237, p85

- Mao S., Schneider P., 1998, MNRAS, 295, 587
- Mao S., Jing Y. P., Ostriker J. P., Weller J. 2004, ApJ, 604, L5
- Moore B., Ghigna S., Governato F. et al., 1999, ApJ, 524, L19
- Oguri M., Lee J., 2004, MNRAS, 355, 120
- Okamoto T., Habe A., 1999, ApJ, 516, 591
- Sheth R. K., 2003, MNRAS, 345, 1200
- Springel V., White S. D. M., Tormen G., Kauffmann G., 2001, MNRAS, 328, 726
- Spergel D.N.S. et al., 2003, ApJS, 148, 175
- Stoehr F., White S. D. M., Springel V., Tormen G., Yoshida N. 2003, MNRAS, 345, 1313
- Taylor J. E., Babul A., 2001, ApJ, 559, 716
- Taylor J. E., Babul A., 2004, MNRAS, 348, 811
- Taylor J. E., Silk J., 2003, MNRAS, 339, 505
- Tormen G., 1997, MNRAS, 290, 411
- Vitvitska M., Anatoly A., Kravtsov A. V., Wechsler R. H., Primack J. R., Bullock J. S., 2002, ApJ, 581, 799
- Warren M. S., Quinn P. J., Salmon J. K., Zurek W. H., 1992, ApJ, 399, 405
- Willman B., Governato F., Dalcanton J. J., Reed D., Quinn T. 2004, MNRAS, 353, 639
- van den Bosch F. C., Lewis G. F., Lake G., Stadel J., 1999, 515, 50
- van den Bosch F. C., Tormen G., Giocoli C., 2005, MNRAS, 359, 1029
- White S. D. M., Rees M. J., 1978, MNRAS, 183, 341
- Zentner A. R., Bullock J. S., 2003, 598, 49
- Zentner A. R., Berlind A. A., Bullock J. S., Kravtsov A. V., Wechsler, R. H., 2005a, ApJ, 624, 505
- Zentner A. R., Kravtsov A. V., Gnedin O. Y., Klypin A. A. 2005b, astro-ph/0502496

Table 1. Halo and subhalo selection parameters: N_{halo} and N_{sub} are the lower limits of the particle number for the host halos and subhalos respectively. The subhalos are selected within a spherical shell from $1 - \Delta r$ to $1 + \Delta r$ in units of the virial radius. The numbers of selected subhalos are listed in the last row.

Model	A	B	C
N_{halo}	500	500	5000
N_{sub}	20	20	20
Δr	0.1	0.2	0.2
number of subhalos	2606	4437	3470

Table 2. Fit parameters for the velocity distributions as defined in eq. (3).

parameter	A	B
a_1	–	–
a_2	2.12	2.62
a_3	2.90	4.48
a_4	–0.333	–0.525
a_5	–0.490	0.238
a_6	1.17	1.20
a_7	0.155	0.140
a_8	–0.564	–0.731
a_9	0.314	0.294

Table 3. Fitting parameters for the density distribution $n_{\text{trri}}(\mu)$ in different mass bins as defined in eq. (6). Each bin is specified by the lower M_l and upper M_u limits of the subhalo mass in units of the mass of the host halo.

	all subhalos	bin 1	bin 2	bin 3	bin 4	bin 5	bin 6
M_u	1	1	0.07943	0.03946	0.02542	0.01709	0.00834
M_l	0.0	0.07943	0.03946	0.02542	0.01709	0.00834	0.0
p0	0.644	0.289	0.259	0.361	0.377	–4.21	–617.8
p1	0.194	6.33×10^{-4}	7.37×10^{-2}	0.159	0.258	4.98	618.8
p2	1.494	9.953	4.281	2.919	2.040	0.130	2.505×10^{-4}

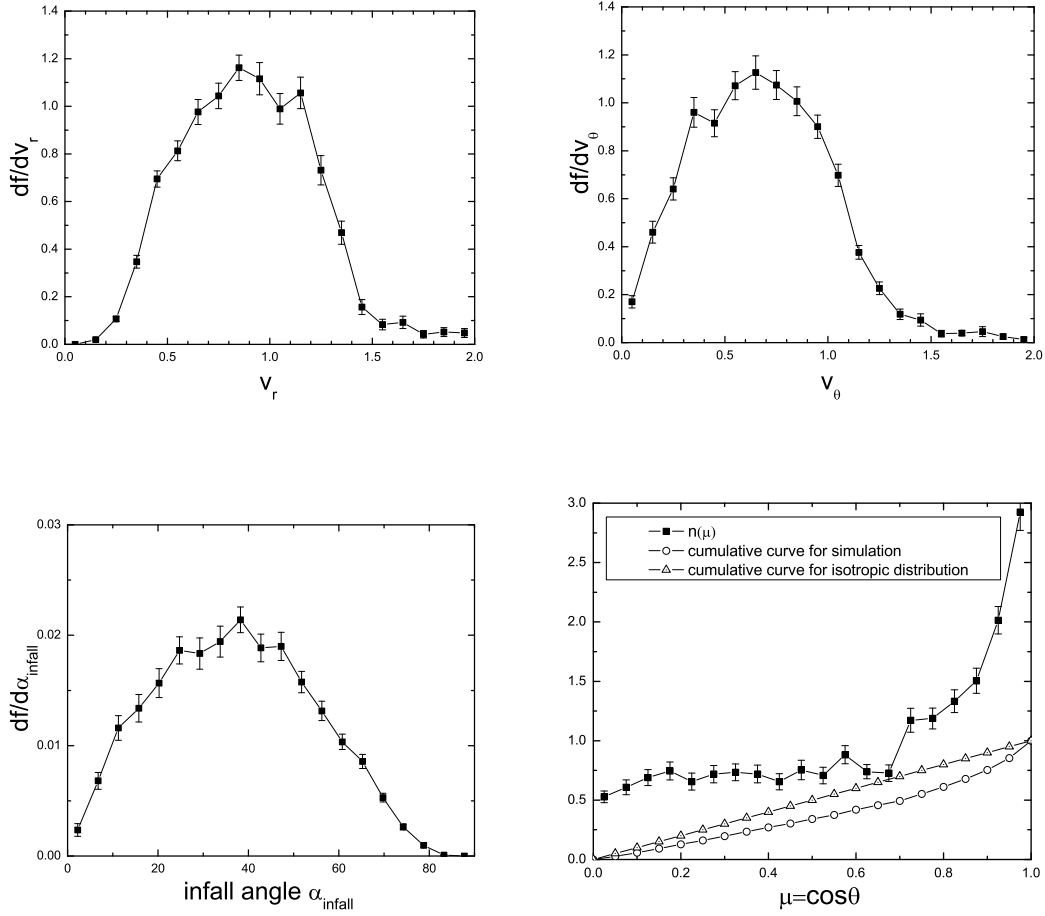


Figure 1. Orbital parameters and spatial distributions for the subhalos selected according to the selection parameter set A in Table 1 in spherical halo model. The upper left and right panels show the distributions of radial and tangential velocities, respectively. The lower left panel shows the distribution of the infall angle, defined in eq. (1). In the lower right-hand panel, fill square shows the distribution of the number density of subhalos per unit area as a function of the angle θ between the vector from the subhalo centre to the host halo centre and the major axis of the host halo. For an isotropic population, the distribution $df/d\mu$ is a horizontal line with amplitude unity. We also show the cumulative distributions for the simulation and an isotropic distribution (open triangles and open circles) in the lower right panel.

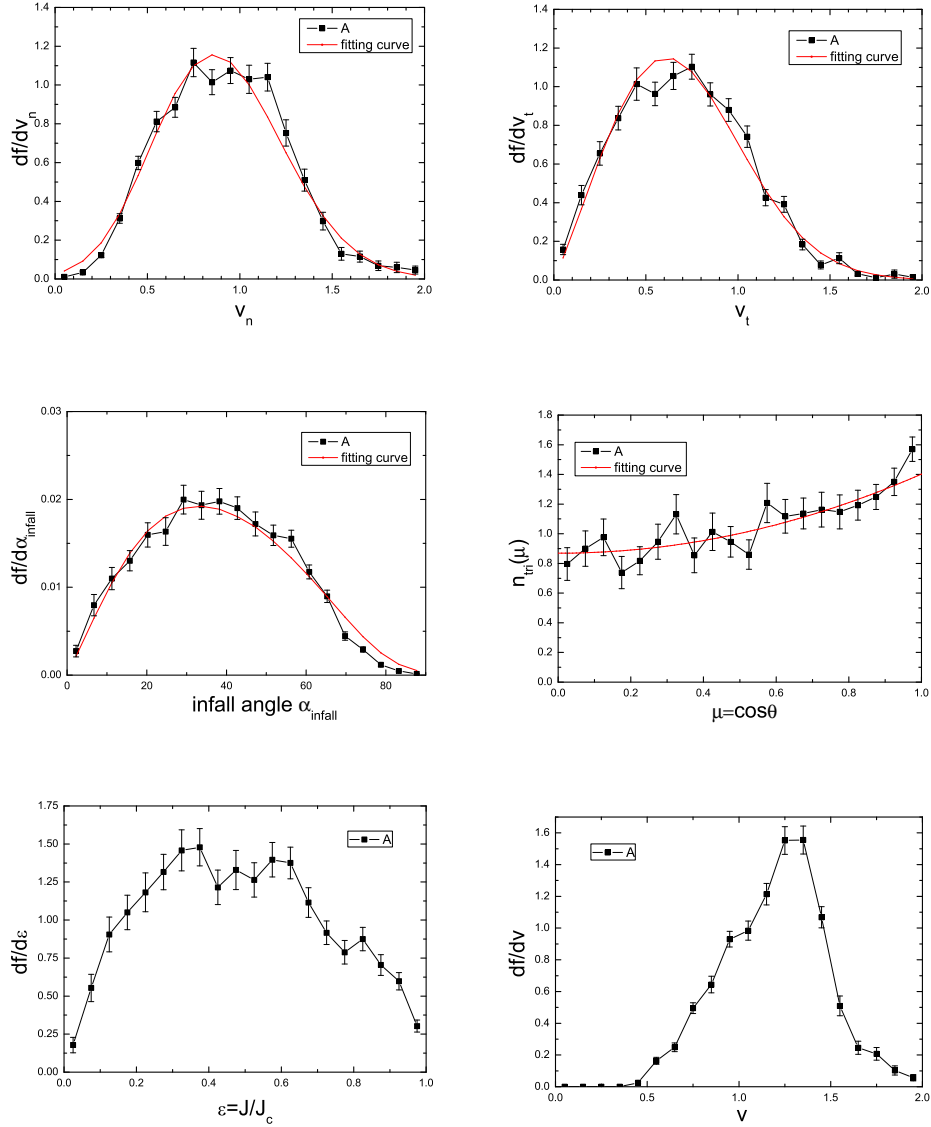


Figure 2. Orbital parameters and spatial distributions for the subhalos selected according to the parameter selection set A in Table 1 in triaxial halo model. The upper left and right panels show the distributions of the normal and tangential velocities respectively. The middle left panel shows the distribution of the infall angle. The middle right panel shows the number density $n_{\text{tri}}(\mu)$ of subhalos at the surface R_{vir} as a function of θ , where θ is the angle between the major axis of the host halo and the vector from the subhalo centre to the host halo centre. The fitting curves as given in eqs. (3) and (6) are shown as a thin line in each panel. The bottom left and right panels show the orbital circularity and the total infall velocity respectively. Notice that the vertical scale in the middle right panel is different from that in the bottom right panel in Fig. 1.

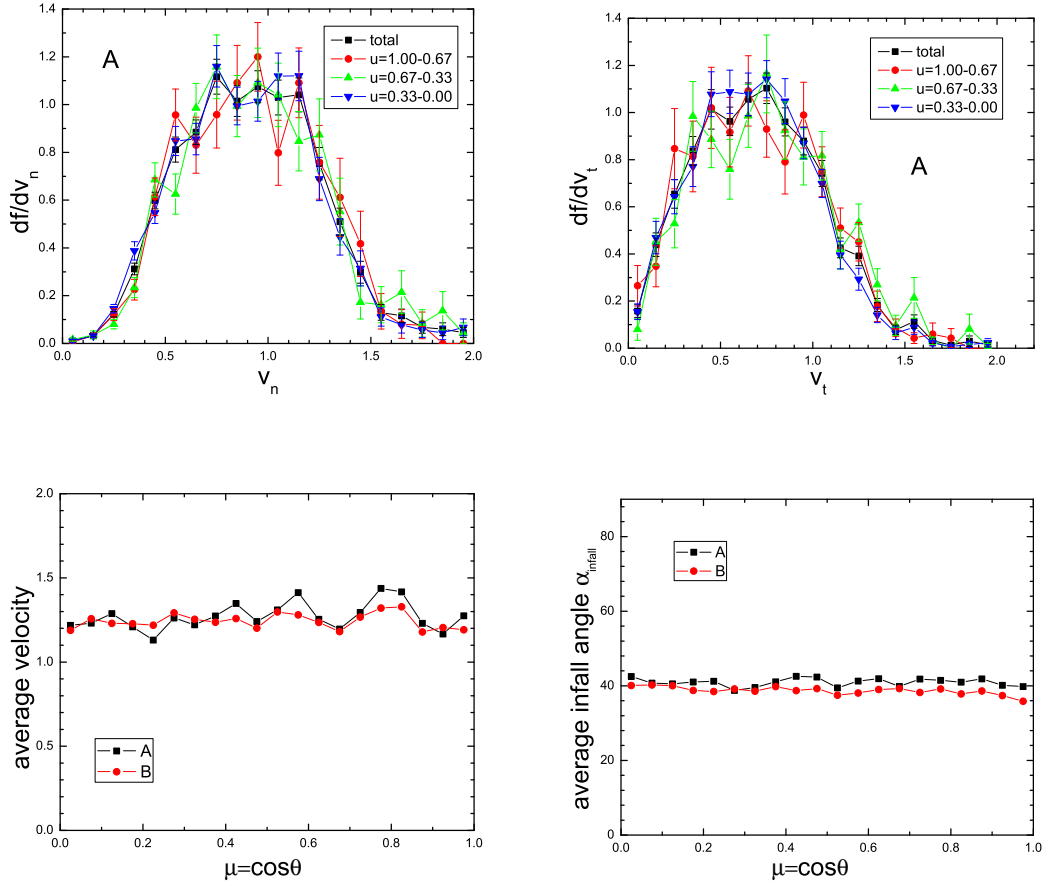


Figure 3. The upper panels plot the distributions of the normal and tangential velocities in different ranges of $\mu = \cos\theta$, where θ is the angle between the vector from the subhalo centre to the host halos centre and the major axis of the host halo. The lower left panel shows the average velocity while the lower right panel shows average infall angle as a function of μ .

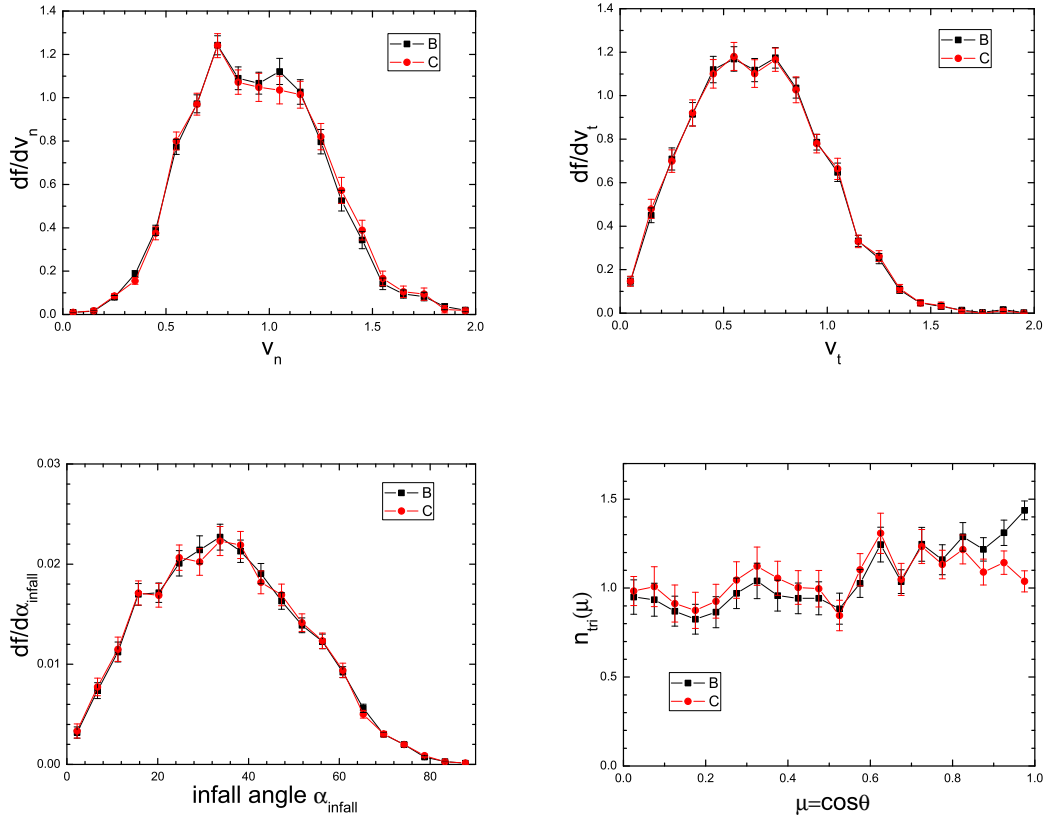


Figure 4. The upper panels show the distributions of the normal and tangential velocities respectively in the triaxial halo model for different subhalo masses (Sets B and C). The lower left panel shows the distribution of the infall angle (α_{infall}) while the lower right panel shows the number density $n_{\text{tr,i}}(\mu)$ of subhalos at the surface R_{vir} , where $\mu \equiv \cos\theta$ and θ is the angle between the major axis of the host halo and the vector connecting the centres of the subhalo and the host halo. The difference between the models B and C in the bottom right panel is due to the different lower limits of the host halo mass (see §3.2).

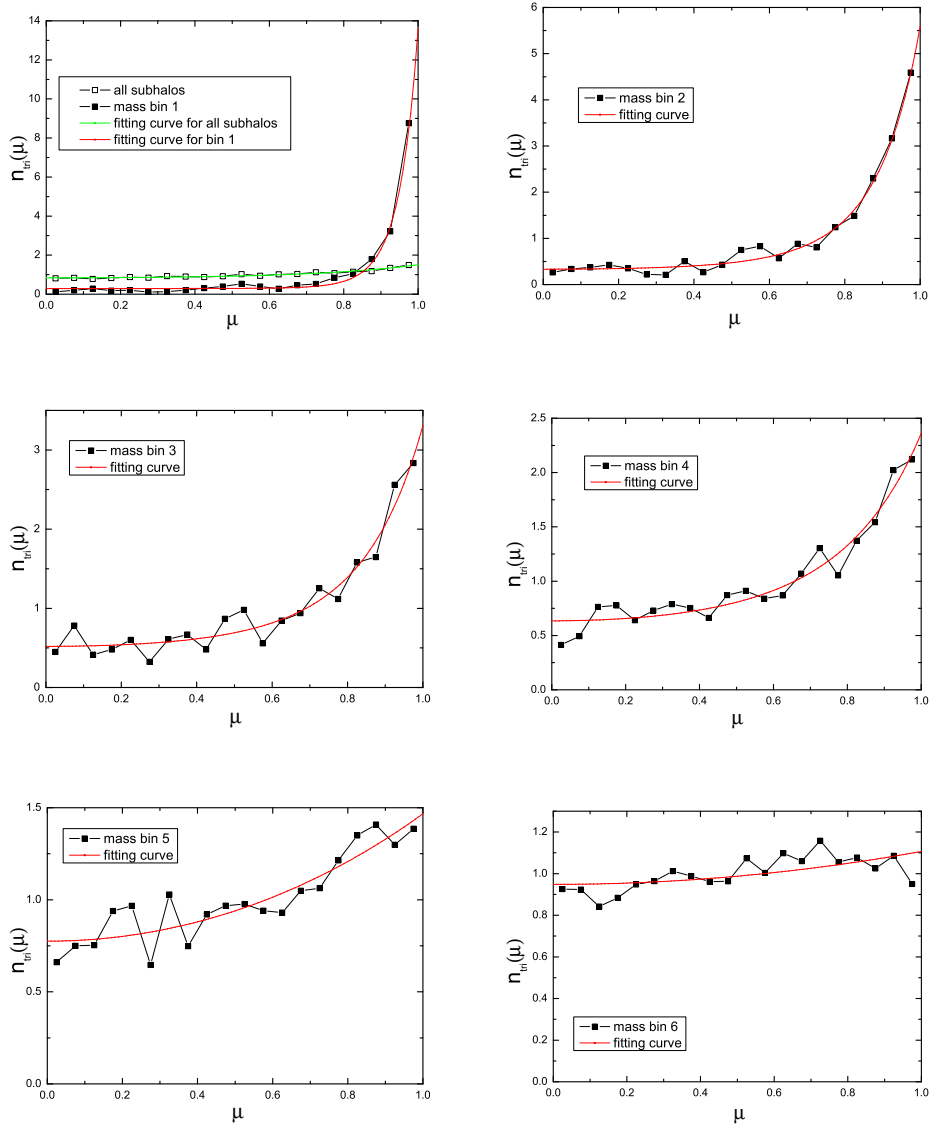


Figure 5. The number density $n_{\text{tri}}(\mu)$ of subhalos at the surface R_{vir} together with the best-fit curves in the triaxial halo model. The subhalos are divided into six bins of $M_{\text{sub}}/M_{\text{host}}$, and the result for each bin is presented in one panel. The mass range for each bin and the corresponding fit parameters (as defined in eq. 6) are listed in Table 3. The distribution for all the subhalos is shown in the top left panel. Notice that the vertical scales are different in different panels.

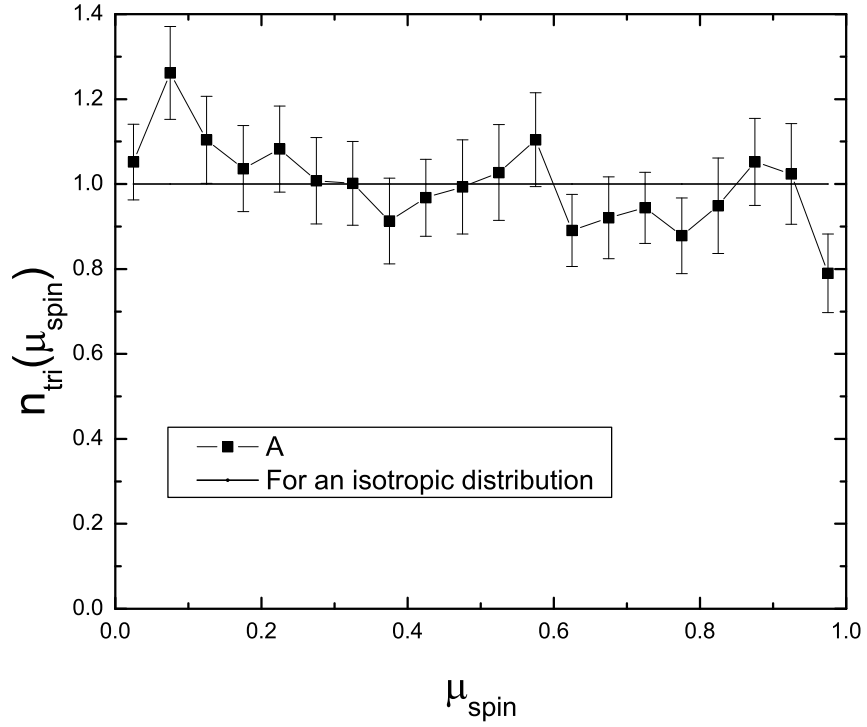


Figure 6. The distribution of $\mu_{\text{spin}} = \cos \theta_{\text{spin}}$ in the tri-axial model, where θ_{spin} is the angle between the spin axis and the line connecting the centres of the parent and satellite halos. The straight line shows the prediction for an isotropic distribution.